Interrelated chemical-microstructural-nanomechanical variations in the structural units of the cuttlebone of Sepia officinalis

L. North, D. Labonte, M. L. Oyen, M. P. Coleman, H. B. Caliskan, and R. E. Johnston

Citation: APL Materials **5**, 116103 (2017);
View online: https://doi.org/10.1063/1.4993202
View Table of Contents: http://aip.scitation.org/toc/apm/5/11
Published by the American Institute of Physics

Interrelated chemical-microstructural-nanomechanical variations in the structural units of the cuttlebone of *Sepia officinalis*

L. North,[1] D. Labonte,[2,a] M. L. Oyen,[2] M. P. Coleman,[1] H. B. Caliskan,[2] and R. E. Johnston[1,a]

[1]*Materials Research Centre, College of Engineering, Swansea University, Swansea SA1 8EN, United Kingdom*

[2]*Cambridge University Engineering Department, Trumpington Street, Cambridge CB2 1PZ, United Kingdom*

(Received 27 June 2017; accepted 16 October 2017; published online 10 November 2017)

"Cuttlebone," the internalized shell found in all members of the cephalopod family *Sepiidae*, is a sophisticated buoyancy device combining high porosity with considerable strength. Using a complementary suite of characterization tools, we identified significant structural, chemical, and mechanical variations across the different structural units of the cuttlebone: the dorsal shield consists of two stiff and hard layers with prismatic mineral organization which encapsulate a more ductile and compliant layer with a lamellar structure, enriched with organic matter. A similar organization is found in the chambers, which are separated by septa, and supported by meandering plates ("pillars"). Like the dorsal shield, septa contain two layers with lamellar and prismatic organization, respectively, which differ significantly in their mechanical properties: layers with prismatic organization are a factor of three stiffer and up to a factor of ten harder than those with lamellar organization. The combination of stiff and hard, and compliant and ductile components may serve to reduce the risk of catastrophic failure, and reflect the role of organic matter for the growth process of the cuttlebone. Mechanically "weaker" units may function as sacrificial structures, ensuring a stepwise failure of the individual chambers in cases of overloading, allowing the animals to retain near-neutral buoyancy even with partially damaged cuttlebones. Our findings have implications for our understanding of the structure-property-function relationship of cuttlebone, and may help to identify novel bioinspired design strategies for lightweight yet high-strength foams. https://doi.org/10.1063/1.4993202

Cuttlefish maintain near-neutral buoyancy at varying diving depths through the use of a specialized floatation device, frequently referred to as cuttlebone, which needs to combine high strength with minimum weight. Despite a porosity exceeding 90%,[1] the cuttlebones of some species withstand pressures encountered at up to 500 m in diving depth.[2–4] This exceptional combination of high compressive strength, porosity, and permeability is extremely desirable for biomimetic and biomedical structural materials, including templates for tissue scaffolds,[5,6] hydroxyapatite scaffolds,[7–9] and bone cements.[10]

The remarkable performance of the cuttlebone is linked to its structural architecture: cuttlebone is composed of calcium carbonate ($CaCo_3$) in its aragonite polymorph with a mixture of β-chitin and other protein complexes, and comprises two main structural units: a dorsal shield and a series of chambers. The continuous chambers are separated by parallel septa and supported by a complex arrangement of meandering plates [from here on referred to as "pillars," see Figs. 1(a)–1(d)].

[a]Authors to whom correspondence should be addressed: r.johnston@swansea.ac.uk and dl416@cam.ac.uk

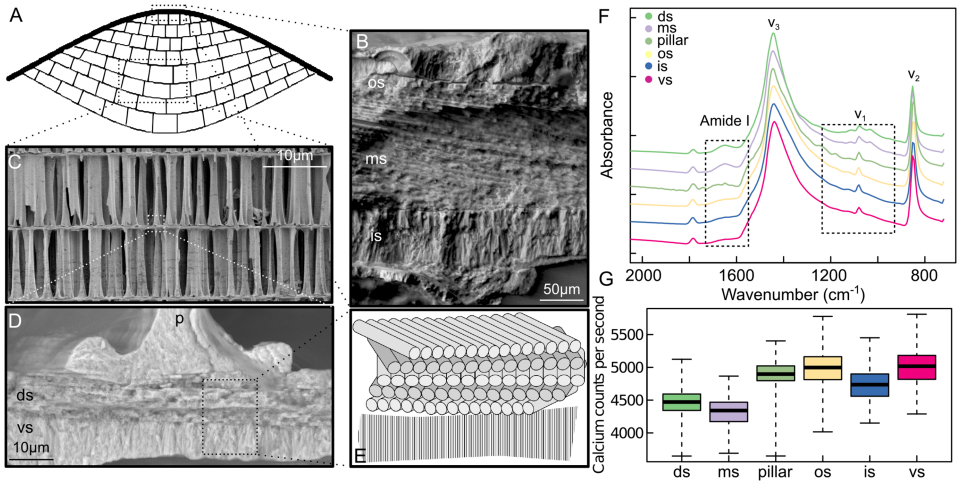

FIG. 1. (a) Schematic cross section of the cuttlebone, indicating the dorsal shield (thick black line) and the chambers (cellular network, thin black lines), which consists of septa and pillars. Scanning electron micrographs of (b) the three distinct layers in the dorsal shield, (c) pillars supporting adjacent chambers, (d) the intersection of a septum and pillar highlighting the different microstructures within a septum. (e) Schematic of the change in direction of fibers in the septum. (f) Chemical analyses of the distinct layered structures in cuttlebone in the form of attenuated total internal reflection (ATR) Fourier Transform Infrared (FTIR) spectra. Each spectrum was normalized and then shifted vertically for clarity. Dashed boxes highlight the aragonite "fingerprint" peak at 1080 cm^{-1} and the presence of organic macromolecules at around 1650 cm^{-1}, respectively. (g) Box-whisker plots illustrating the variation in calcium content between the three layers within the dorsal shield and the two layers within septa, as measured with energy dispersive X-ray spectroscopy (EDS). FTIR and EDS reveal clear differences in the amount of organic matter and the calcium content between the layers of both the dorsal shield and septa, which are similar among prismatic and lamellar crystal organizations, respectively. p—pillar, os—outer shield, ms—middle shield, is—inner shield, ds—dorsal septum, and vs—ventral septum.

The macro-structure,[1,11–14] growth mechanisms,[11,15] bulk mechanical performance,[1,4,12,16] and chemical composition of cuttlebone,[17] as well as the role of the organic constituents in the formation of the chambers and the organization of the crystals have been studied in some detail.[1,11,15,17,18] However, the structure-property relationships across the identified structural units of this complex biomaterial have not yet been fully investigated (but see Refs. 1,4,16,19–21), although these units were first identified more than 180 years ago.[22] In this work, we aim to close this gap and provide a detailed chemical, structural, and mechanical analysis of the different structural units, using scanning electron microscopy (SEM), energy dispersive X-ray spectroscopy (EDS), Fourier transform infrared spectroscopy (FTIR), and nanoindentation.

Fresh specimens of *Sepia officinalis* Linnaeus, 1758, were acquired commercially from around the UK coastline. The cuttlebone was dissected, sectioned into smaller samples (approximately 2 cm^3) taken from the central region of the cuttlebone, and embedded in epoxy resin (EpoFix, Struers) using vacuum impregnation. Embedded specimens were diamond and colloidal silica polished to 0.04 μm finish, and a 7 nm carbon coating was applied using a Quorum Technologies Q150T turbo-pumped carbon coater.

EDS analysis in the form of line scans at 10 kV was carried out on transverse sections to provide information on the calcium content of both the dorsal shield and the chambers, using a Carl Zeiss Crossbeam 540 FEG SEM equipped with an SMax50 EDS detector, controlled via the Aztec software (Oxford Instruments). 10 line scans were performed with sampling separations within each line of 3.3 μm and 0.14 μm for the dorsal shield and the septa, and 6 line scans with sampling separations of 2.4 μm for the pillars, respectively; each line was measured three times and the arithmetic mean was used in further analyses.

Spectroscopic analysis of the samples was conducted using a PerkinElmer Spotlight400 FTIR fitted with an attenuated total internal reflection (ATR) imaging mode microscope (PerkinElmer, Waltham, Massachusetts, USA). The wavelength resolution was set to 12 cm^{-1}, and eight scans per pixel were collected, with a pixel size of 1.56 μm.

Mechanical properties of the different structural units of the cuttlebone were measured in ambient conditions with a TI 950 Triboindenter (Hysitron, Eden Prairie, USA), equipped with a diamond Berkovich indenter with a tip radius of 150 nm. Indentations were conducted in closed-loop displacement-control with a 5-10-5 s load-hold-unload trapezoidal load profile, and a peak displacement of 200 nm unless stated otherwise. Indentation hardness (H) and indentation modulus (E') were extracted from the force-displacement data using the Oliver and Pharr method.[23] In order to quantify the variation in H and E' across the shield, 18 horizontal (orthogonal to the dorso-ventral axis) lines of 25 vertical (along the dorso-ventral axis) indents were placed across the shield of one specimen, starting on the septum adjacent to the ventral layer of the shield, and finishing on the surrounding epoxy. The vertical and horizontal spacings were 20 μm and at least 20 μm, respectively. The results were averaged either according to their vertical position for plotting, or according to "region" for further statistical analyses.

The mechanical properties of 14 randomly selected pillars were measured at various points along their length. The exact position varied across the pillars due to variable cross-sectional width, and we avoided regions that were thin or close to air gaps; the minimum vertical spacing was 20 μm. A linear regression of H and E' against the indentation position normalized by pillar length revealed that neither differed significantly along the length of the pillars (t-test for the slope, t-statistic = 0.40, p-value = 0.69 and t-statistic = 0.61, p-value = 0.52 for E′ and H, respectively). In order to capture the variation of material properties across pillars, 35 further pillars were indented, with three indents per pillar, located approximately at the bottom, middle, and top relative to the pillar length. All results were pooled for further analyses.

Preliminary microscopy of the septum suggested that it contained at least two distinct regions [see Figs. 1(d)], separated roughly at the midline [see also Refs. 15 and 18]. In order to quantify the properties of these two regions, 60 indents were placed approximately centrally in each region, with a horizontal spacing of at least 20 μm. In addition, we used the accelerated property-mapping (XPM) feature of the Triboindenter to visualize localized changes in material properties. XPM measurements were conducted in force-control, as recommended by the manufacturer. Mechanical properties of the shield were mapped with a 3 × 148 (3 μm vertical × 3 μm horizontal spacing) grid, a peak load of 1 mN, and a 1-2-1 s trapezoidal load profile. The variation in mechanical properties at the transition between pillar and septum was visualized with a 12 × 25 (5 μm horizontal × 2 μm vertical) grid, with a peak load of 0.8 mN, and a 1-5-1 s trapezoidal loading profile. Only measurements with a contact depth exceeding 60 nm were used for further analyses, and data excluded by this criterion were linearly interpolated from the surrounding data points. All XPM data were used for plotting mechanical property maps and were not included in the quantitative statistical analysis.

The main structural components of the cuttlebone—the dorsal shield, the septa, and the pillars—can be readily identified by light and electron microscopy (Fig. 1). The dorsal shield consists of two layers formed of prismatic tubercles that encapsulate a middle layer with lamellar aragonite structure [Fig. 1(b) and Ref. 13]. This difference is also apparent in backscattered electron imaging, where the sandwiched layer shows a reduced atomic density [see Fig. S1(a) of the supplementary material]. A similar structural arrangement was found for the septa, which are split at about midline [Figs. 1(d) and 1(e)], confirming previous work, which has shown that the dorsal part of the septa has an aragonite lamella-fibrillar microstructure with fibers oriented in multiple directions on different planes.[15,24] The prismatic structure of the ventral part, in turn, consists of aragonite fibers oriented parallel to the pillar height, which are crystallographically continuous into the adjacent pillar [Figs. 1(d) and 1(e)].

These structural differences were also evident in both FTIR spectra and EDS data. While the "fingerprint" peaks of aragonite were present in all spectra, components with a lamellar ultrastructure showed a distinct broadening of the v1-mode peak (1080 cm^{-1}), and additional low-intensity peaks between 1000 and 1300 cm^{-1} as well as at 1650 cm^{-1}, indicative of the presence of a significant amount of organic macromolecules [Fig. 1(f)].[18] Components with a prismatic morphology, in turn, had a larger Ca count per second (cps), as measured via EDS [4915 ± 16.1 compared to 4392 ± 10.75 cps, for detailed data on individual layers, see Fig. 1(g) and Table SI of the supplementary material]. This difference translated into calcium weight percentages of 46.5% for the prismatic and 45.15% for the lamellar components.

While these differences may sound minor, in combination they lead to a marked difference in mechanical properties. Nanoindentation revealed that units with prismatic structure have an indentation modulus which exceeds that of lamellar components by a factor between two and three, and an indentation hardness which is up to a factor of ten larger (see Figs. 2 and 3 and Table SI of the supplementary material for detailed data). For both the dorsal shield and the septa, the changes in material properties between prismatic and lamellar building blocks appear to be abrupt and occurred on a microscopic length scale, as evident from the XPM [see Figs. 2(c) and 3, respectively]. Note that the ventral septa and the outer shield have a similar chemical composition but vary in indentation modulus and hardness, likely due to edge effects arising from the narrow width of the ventral septum (<10 μm).

Cuttlebone needs to be as light as possible to maximize buoyancy but as strong as necessary to ensure sufficient safety factors. These conflicting demands are reflected in a complex bio-architecture, featuring at least six different structural units, which differ not only in their microstructure and chemical composition, but also in their mechanical properties (see Figs. 1–3). Stiff and hard layers with prismatic crystal organization alternate with more compliant and ductile zones, organized in a lamellar form and enriched with organic macromolecules. The inclusion of "weaker" layers may at first seem surprising, as the maximum diving depth is directly related to the mechanical properties for

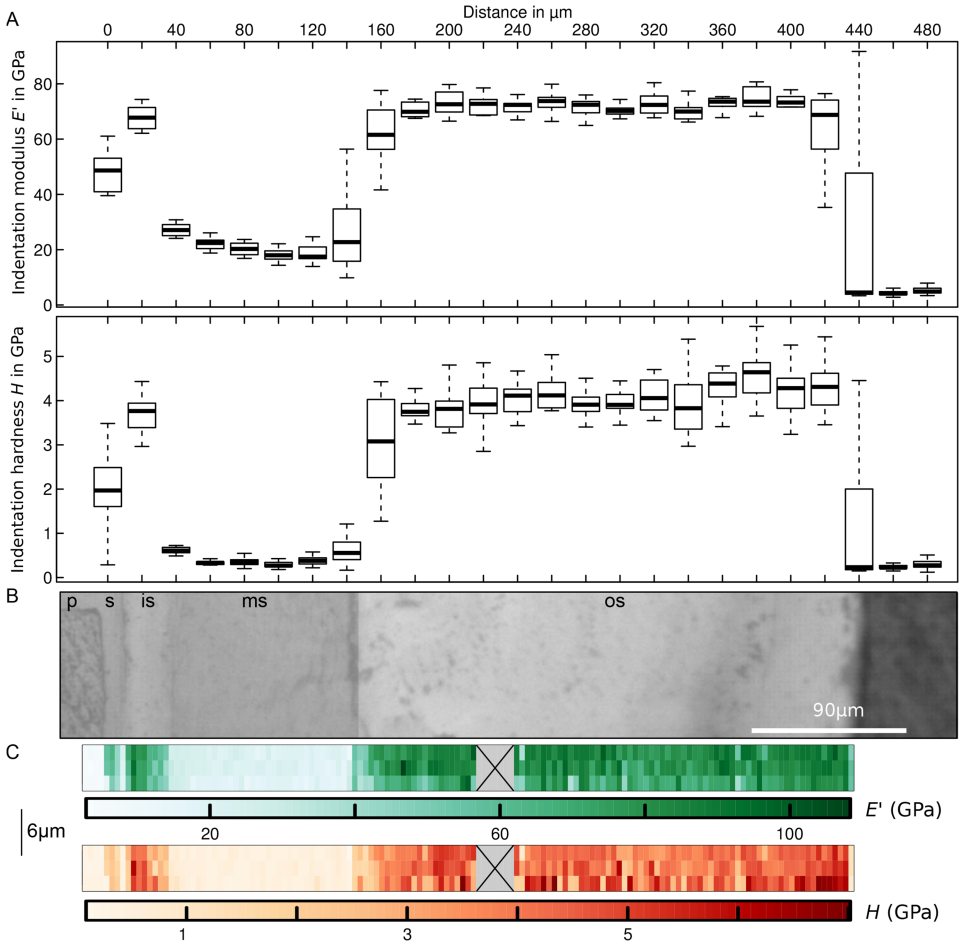

FIG. 2. (a) Box-whisker plots illustrating the variation in indentation modulus and hardness across the different layers in the dorsal shield, which are shown in the light microscopy image in (b) (n = 18 per box-whisker plot). The clear differences in indentation hardness and modulus and the sharp transition between the different layers are visualized further in (c), which shows data collected with the accelerated property mapping feature of the 950 Triboindenter. The crossed-out, grey block in (c) is an unmapped region. p—pillar, os—outer shield, ms—middle shield, is—inner shield, s—septum.

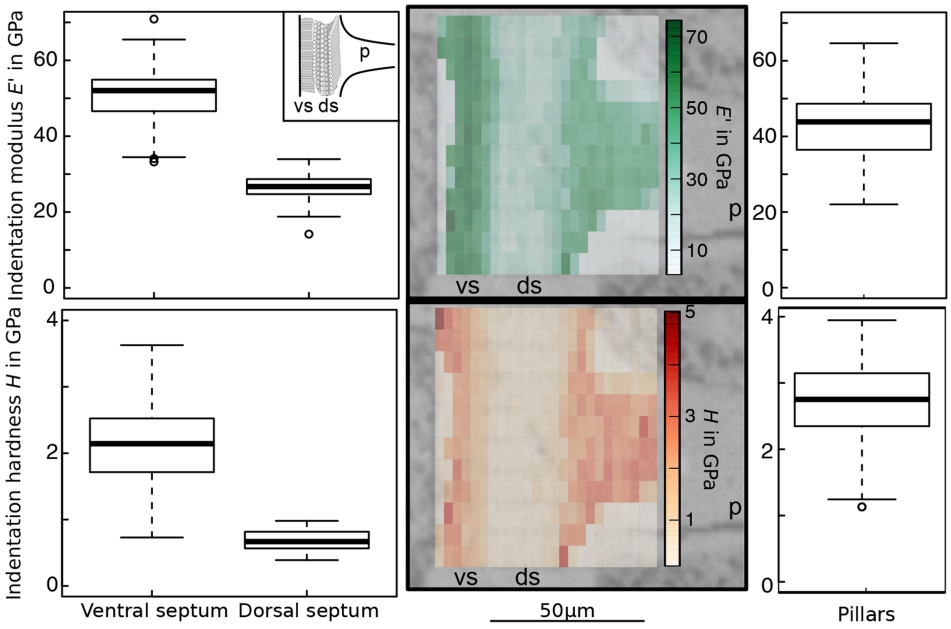

FIG. 3. Box-whisker plots illustrating the variation in indentation modulus and hardness in the two distinct layers in the septa (left-hand side, n = 60 per layer) and the pillars (right-hand side, n = 275 for 49 different pillars). The clear differences in indentation hardness and modulus and the apparent sharp transition between the different layers are visualized further in the central region of the figure, which shows data collected with the accelerated property mapping feature of the 950 Triboindenter, overlaid on an light microscopy image of the corresponding region. p—pillar, ds—dorsal septum, vs—ventral septum.

a given geometric arrangement.[4,12] However, several arguments may be brought forward to rationalize this design strategy.

First, variations in indentation modulus between adjacent layers may represent a toughening mechanism. Cracks are effectively arrested at the interface between adjacent layers if the ratio of their elastic moduli is greater than about 5,[25] as, for example, observed in hexactinellid sponges,[26] albeit at a much smaller scale. Similar mechanisms have also been described for nacre,[25,27,28] again at a much smaller scale than described here. Both the middle layer of the dorsal shield and the dorsal septum might be particularly effective in arresting cracks, as they have an unusually small ratio between indentation hardness and modulus (about half of 0.05, the value typical for biological materials), which is a proxy for the tendency of a material to undergo elastic versus inelastic deformation.[29] Hence, these layers may absorb energy by inelastic deformation instead of feeding it into the propagation of cracks. Indeed, X-ray microCT investigation of the dorsal shield revealed several cases where cracks seemingly originating in the outer shield failed to penetrate the central layer of the shield, and instead were arrested at the interface, providing support for our hypothesis [see Fig. S1(c) of the supplementary material].

Second, and related to the first point, the inclusion of "sacrificial" layers may represent a strategy to ensure controlled and localized structural failure in case of overloading, for example, by directing gross failure to the pillars. The question remains, however, which failure mechanism would be most beneficial for the organism. Overloaded pillars collapse, resulting in a stepwise failure and densification of individual chambers [see Fig. S1(b) of the supplementary material for a 4D X-ray microtomography visualization]. Cuttlefish can survive multiple of such chamber failures,[3] and the variation in mechanical properties identified in this study might be key to avoid a damaging through-thickness crack in the dorsal shield, which would compromise near-neutral buoyancy.

Third, the proteinous organic matrix plays a major role in cuttlebone formation,[15,18,30] so that variations in the amount of organic molecules might simply reflect a developmental pattern rather than a mechanical adaptation.

The way in which the cuttlebone fails when overloaded also has implications for the link between cuttlebone morphology and maximum diving depth established by earlier work.[2–4] Previous studies have used beam or plate theory to study the mechanical performance of the *Sepia* cuttlebone with reasonable success.[4,12] While these studies assumed that failure occurs via elastic buckling of the pillars, there are two other competitive failure modes in foam-like solids, "plastic" collapse, or brittle crushing.[31] Notably, the maximum sustainable stress, σ, predicted for the two latter failure modes is directly proportional to the aspect ratio characterizing the repetitive unit, which we define here as wall thickness, *t*, versus wall length, *l*. In contrast, $\sigma \sim (t/l)^2$ for elastic buckling[31] implying that elastic buckling will be the dominant failure mode for structures with small aspect ratios (see supplementary material). However, for animals which dive to deeper depths—and hence typically possess chambers with larger aspect ratios[4]—the mechanical performance limit might be set by plastic collapse or brittle crushing instead, and indeed the "frayed" failure of some cuttlebone under compression suggests that brittle crushing may be dominant.[1,16]

The identified variations in ultrastructure, chemistry, and mechanical properties across the structural units of the cuttlebone are not only relevant for our understanding of the structure-function relationship in the cuttlebone, but also for the design of bioinspired foams which combine low weight with high strength.

See supplementary material for a summary of the mechanical property data, further electron microscopy, X-ray microCT of layer failure, and a description of possible cuttlebone failure based on a foam model.

The work was supported by the Advanced Imaging of Materials (AIM) facility (EPSRC Grant No. EP/M028267/1), the European Social Fund (ESF) through the European Union's Convergence programme administered by the Welsh Government, the United States Army Corps of Engineers, Engineer Research and Development Centre (ERDC), the Denman Baynes Senior Research Fellowship (to D.L.), the Islamic Development Bank & the Cambridge Commonwealth, European and International Trust PhD Scholarship (to H.B.C.), and an EPSRC Doctoral Training Award (EPSRC Grant No. EP/K502935/1 to L.N.). The authors would like to thank Peter Davies for microscopy technical assistance and Dr. Ed Pope for discussions on *Sepia officinalis* behavior. All data created during this research are openly available from the Swansea University data archive at https://doi.org/10.5281/zenodo.1039667.

[1] J. D. Birchall and N. L. Thomas, "On the architecture and function of cuttlefish bone," J. Mater. Sci. **18**(7), 2081–2086 (1983).
[2] P. D. Ward and S. V. Boletzky, "Shell implosion depth and implosion morphologies in three species of Sepia (Cephalopoda) from the Mediterranean Sea," J. Mar. Biol. Assoc. U. K. **64**(4), 955 (1984).
[3] P. Neige and S. V. Boletzky, "Morphometrics of the shell of three Sepia species (Mollusca: Cephalopoda): Intra-and interspecific variation," Zool. Beitr. **38**, 137–156 (1997).
[4] K. Sherrard, "Cuttlebone morphology limits habitat depth in eleven species of Sepia (Cephalopoda: Sepiidae)," Biol. Bull. **198**(3), 404–414 (2000).
[5] J. H. G. Rocha, A. F. Lemos, S. Agathopoulos, P. Valerio, S. Kannan, F. N. Oktar *et al.*, "Scaffolds for bone restoration from cuttlefish," Bone **37**(6), 850–857 (2005).
[6] W. Ogasawara, W. Shenton, S. A. Davis, and S. Mann, "Template mineralization of ordered macroporous chitin–silica composites using a cuttlebone-derived organic matrix," Chem. Mater. **12**(10), 2835–2837 (2000).
[7] H. Ivankovic, G. G. Ferrer, E. Tkalcec, S. Orlic, and M. Ivankovic, "Preparation of highly porous hydroxyapatite from cuttlefish bone," J. Mater. Sci.: Mater. Med. **20**(5), 1039–1046 (2009).
[8] D. Milovac, G. Gallego Ferrer, M. Ivankovic, and H. Ivankovic, "PCL-coated hydroxyapatite scaffold derived from cuttlefish bone: Morphology, mechanical properties and bioactivity," Mater. Sci. Eng., C **34**, 437–445 (2014).
[9] E. Battistella, S. Mele, I. Foltran, I. G. Lesci, N. Roveri, P. Sabatino *et al.*, "Cuttlefish bone scaffold for tissue engineering: A novel hydrothermal transformation, chemical-physical, and biological characterization," J. Appl. Biomater. Funct. Mater. **2**(10), 99–106 (2012).
[10] S. García-Enriquez, H. E. R. Guadarrama, I. Reyes-González, E. Mendizábal, C. F. Jasso-Gastinel, B. García-Enriquez *et al.*, "Mechanical performance and *in vivo* tests of an acrylic bone cement filled with bioactive *Sepia officinalis* cuttlebone," J. Biomater. Sci., Polym. Ed. **21**(1), 113–125 (2010).
[11] K. Tanabe, Y. Fukuda, and Y. Ohtsuka, "New chamber formation in the cuttlefish *Sepia esculenta* Hoyle," Venus **44**, 55–67 (1985).
[12] D. Gower and J. F. V. Vincent, "The mechanical design of the cuttlebone and its bathymetric implications," Biomimetics **4**, 37–58 (1996).
[13] J. J. A. Appellöf, *Die Schalen Von Sepia, Spirula Und Nautilus: Studien Über Den Bau Und Das Wachsthum* (PA Norsted & Söner, 1893), Vol. 25.

[14] K. Bandel and S. V. Boletzky, "Comparative study of the structure, development and morphological relationships of chambered cephalopod shells," Veliger **21**(3), 313 (1979).
[15] A. G. Checa, J. H. E. Cartwright, I. Sánchez-Almazo, J. P. Andrade, and F. Ruiz-Raya, "The cuttlefish *Sepia officinalis* (Sepiidae, Cephalopoda) constructs cuttlebone from a liquid-crystal precursor," Sci. Rep. **5**(1), 11513 (2015).
[16] S. A. Tekalur, M. Raetz, and A. Dutta, "Composite design through biomimetic inspirations," in *Experimental and Applied Mechanics*, edited by T. Proulx (Springer, New York, NY, 2011), Vol. 6, pp. 355–357.
[17] M. Florek, E. Fornal, P. Gómez-Romero, E. Zieba, W. Paszkowicz, J. Lekki *et al.*, "Complementary microstructural and chemical analyses of *Sepia officinalis* endoskeleton," Mater. Sci. Eng., C **29**(4), 1220–1226 (2009).
[18] C. Le Pabic, A. Marie, B. Marie, A. Percot, L. Bonnaud-Ponticelli, P. J. Lopez *et al.*, "First proteomic analyses of the dorsal and ventral parts of the *Sepia officinalis* cuttlebone," J. Proteomics **150**, 63–73 (2017).
[19] J. Cadman, S. Zhou, Y. Chen, W. Li, R. Appleyard, and Q. Li, "Characterization of cuttlebone for a biomimetic design of cellular structures," Acta Mech. Sin. **26**(1), 27–35 (2010).
[20] J. Cadman, C.-C. Chang, J. Chen, Y. Chen, S. Zhou, W. Li *et al.*, "Bioinspired lightweight cellular materials—Understanding effects of natural variation on mechanical properties," Mater. Sci. Eng., C **33**(6), 3146–3152 (2013).
[21] A. Knöller, T. Runčevski, R. E. Dinnebier, J. Bill, and Z. Burghard, "Cuttlebone-like V_2O_5 nanofibre scaffolds—Advances in structuring cellular solids," Sci. Rep. **7**, 42951 (2017).
[22] E. Griffith and E. Pidgeon, "The Mollusca and Radiata," in *Arranged by the Baron Cuvier, with Supplementary Additions to Each Order* (Whittaker and Company, London, 1834).
[23] W. C. Oliver and G. M. Pharr, "An improved technique for determining hardness and elastic modulus using load and displacement sensing indentation experiments," J. Mater. Res. **7**(6), 1564–1583 (1992).
[24] L. A. Doguzhaeva and E. Dunca, "Siphonal zone structure in the cuttlebone of *Sepia officinalis*," Swiss J. Palaeontol. **134**(2), 167–176 (2015).
[25] P. Fratzl, H. S. Gupta, F. D. Fischer, and O. Kolednik, "Hindered crack propagation in materials with periodically varying Young's modulus—Lessons from biological materials," Adv. Mater. **19**(18), 2657–2661 (2007).
[26] J. Aizenberg, J. C. Weaver, M. S. Thanawala, V. C. Sundar, D. E. Morse, and P. Fratzl, "Skeleton of *Euplectella* sp.: Structural hierarchy from the nanoscale to the macroscale," Science **309**(5732), 275–278 (2005).
[27] H. Kakisawa and T. Sumitomo, "The toughening mechanism of nacre and structural materials inspired by nacre," Sci. Technol. Adv. Mater. **12**(6), 64710 (2011).
[28] O. Kolednik, J. Predan, F. D. Fischer, and P. Fratzl, "Bioinspired design criteria for damage-resistant materials with periodically varying microstructure," Adv. Funct. Mater. **21**(19), 3634–3641 (2011).
[29] D. Labonte, A.-K. Lenz, and M. L. Oyen, "On the relationship between indentation hardness and modulus, and the damage resistance of biological materials," Acta Biomater. **57**, 373–383 (2017).
[30] V. Čadež, S. D. Škapin, A. Leonardi, I. Križaj, S. Kazazić, B. Salopek-Sondi *et al.*, "Formation and morphogenesis of a cuttlebone's aragonite biomineral structures for the common cuttlefish (*Sepia officinalis*) on the nanoscale: Revisited," J. Colloid Interface Sci. **508**, 95–104 (2017).
[31] L. J. Gibson and M. F. Ashby, *Cellular Solids: Structure and Properties*, Cambridge Solid State Science Series, 2nd ed. (Cambridge University Press, Cambridge, 2001), p. 510, 1. Paperback ed. (with corr.), transferred to digital printing.